Lawrence Berkeley National Laboratory

Title
Synthesis and Characterization of Non-Aqueous [TcXM-PW11O39]n– with M = O, N: Comparing TcV and TcVI in Metal Oxide Matrices

Permalink

Journal

ISSN

Authors
Burton-Pye, Benjamin P
Dembowski, Mateusz
Lukens, Wayne W
et al.

Publication Date

DOI

Peer reviewed

Regarding the synthesis and characterization of keggin ions incorporating TcX³⁺ cores

Benjamin P. Burton-Pye[1,2], Mateusz Dembowski[3†], Wayne W. Lukens Jr.[4],*

Anthony Cruz[1,2], Alrasheed Althour, Jasmine Hatcher[2,3], Julie Bertoia[5], Gustavo

Lopez[1,2], Donna McGregor[1,2] and Lynn C. Francesoni[2,3]*

[1]Lehman College of the City University of New York, 250 Bedford Park Boulevard West, Bronx, NY 10468

[2]Ph.D. Program in Chemistry, Graduate Center of the City University of New York, New York, NY 10016, USA

[3]Hunter College of the City University of New York, 695 Park Avenue, New York, NY 10065, USA

[4]Chemical Sciences Division, The Glenn T. Seaborg Center, E.O. Lawrence Berkeley National Laboratory (LBNL), One Cyclotron Road, Berkeley, California 94720, USA

[5]Department of Chemistry, University of Nevada Las Vegas, Las Vegas, Nevada 89154, USA

KEYWORDS (Word Style "BG_Keywords"). Technetium, polyoxometalate, EXAFS, XANES, DFT

ABSTRACT (Word Style "BD_Abstract"). All manuscripts must be accompanied by an abstract. The abstract should briefly state the problem or purpose of the research, indicate the theoretical or experimental plan used, summarize the principal findings, and point out major conclusions. Abstract length is one paragraph.

Introduction

Technetium (^{99}Tc, $t_{1/2}$ = 211 ka) is fission product with multiple oxidation states that complicate our understanding of its behavior in nuclear waste as well as in the environment.{Icenhower, 2010 #35}{Burke, 2005 #18}{Ishii, 2006 #36} Its stable form in aerobic conditions, TcO_4^-, is environmentally mobile and does not sorb well to mineral surfaces. One of the key challenges to understanding the environmental chemistry of this element is predicting its chemical speciation in reducing environments, particularly in the presence of ligands that can complex reduced technetium.{Gu, 2011 #31} {Boggs, 2011 #13}

To that end, the interaction of technetium with ferrous minerals has been studied extensively. These studies have shown that pertechnetate is reduced by the mineral and may be adsorped onto the mineral surface or replace Fe(III) in the crystalline lattice.{Fredrickson, 2004 #28}{Fredrickson, 2004 #28;Fredrickson, 2009 #29}{Farrell, 1999 #27}{Kobayashi, 2013 #44} {Marshall, 2014 #61}{Yalcintas, 2016 #111}{Yalcintas, 2015 #112} In either case, the reduced form of technetium has much lower environmental mobility than TcO_4^-. In the absence of other ligands, including mineral surfaces, the main form of the reduced technetium is $TcO_2.xH_2O$, which slowly oxidizes to TcO_4^- in the presence of oxygen.{Cartledg.G., 1971 #19} In the environment, reduced technetium is sometimes resistant to reoxidation and mobilization while reduced technetium in other samples show considerable resistance to oxidation.{Burke, 2006 #17;Burke, 2005 #18}{Morris, 2008 #66} It is therefore clear, that in order to understand the behavior of technetium in environments with varying electrochemical potentials, a molecular level understanding of the reduced forms is needed.

A way that our group has approached to bridge this gap of knowledge is to study technetium within the bonds of a family of soluble metal oxide matrices called polyoxometalates (POMs). POMs are transition metal-oxide clusters that are excellent models for mineral surfaces. They are structurally simple, robust molecular scaffolds that can complex a wide range of metal atoms in many oxidation states[1-4]. The advantage of soluble metal oxide system, such as POMs, is that they can be studied at the molecular level by a

number of species-specific techniques. We have shown that TcO_4^- can be reduced and incorporated into α_2-$P_2W_{17}O_{61}^{10-}$ via a photo-activated reduction mechanism.[5] The technetium is incorporated into surface sites the α_2-$P_2W_{17}O_{61}^{10-}$ framework as a $Tc^V=O$. Electrochemically this compound has a wide redox stability over a wide pH range and may provide insight to the chemical environment of Tc incorporated into other mineral defect sites.

In this study, we have revisited the Keggin POM systems first reported by Abrams et al[6] in organic media. We report the extended characterization of $TBA_4[Tc^VO\text{-}PW_{11}O_{39}]$, $TBA_4[Tc^{VI}N\text{-}PW_{11}O_{39}]$, including cyclic voltammetry, multinuclear NMR, mass spectrometry and EXAFS and XANES. We also explore the chemical generation of $TBA_3[Tc^{VI}O\text{-}PW_{11}O_{39}]$.

Experimental Section

General. *Caution! ^{99}Tc is a weak β- emitter with a half-life of 2.1 x 10^5 years. All syntheses were performed in a laboratory approved for low-level use of radioactivity using appropriate radioactive material handling procedures.* All materials were purchased as reagent grade and used without further purification. Solid ammonium pertechnetate (NH_4TcO_4) was purchased from Oak Ridge National Laboratory. Water was obtained using a Millipore Direct Q5 system (conductivity =18 mΩ). NH_4TcO_4 becomes contaminated with TcO_2 due to radiolytic auto-reduction and is black in color; pure NH_4TcO_4 is a white crystalline solid. To regenerate pure pertechnetate the raw NH_4TcO_4 was dissolved in water and heated with hydrogen peroxide[7] until the volume

had decreased by half. The resulting colorless aqueous solution was standardized using a well-established UV-Vis protocol. (TBA)TcOCl$_4$ and (TBA)TcNCl$_4$ were prepared from NH$_4$TcO$_4$ according to established procedures. [8]

Collection of NMR Data. NMR spectra of solutions were collected at 298K on a BRUKER Ascend-400 spectrometer with 5 mm tubes fitted with Teflon inserts that were purchased from Wilmad Glass. The resonance frequencies of ^{31}P and ^{183}W on this spectrometer are 161.99 and 16.67 MHz respectively. Typical acquisition parameters for ^{31}P spectra include the following: spectral width 20 kHz; acquisition time, 1.6 s; pulse delay 0.5 s, and pulse width 11µs. Typical acquisition parameters for ^{183}W spectra include the following: spectral width 3.3 kHz; acquisition time, 9.8 s; pulse delay 1.0 s, and pulse width 100µs.

Extended X-Ray Absorption Fine Structure (EXAFS) Spectroscopy. Each sample was transferred to polypropylene centrifuge tube and sealed inside a polyethylene pouch, which was sealed inside a polyester bag. Data were obtained at SSRL BL 11-2 at room temperature. X-rays were monochromatized using a double crystal monochromator with Si 220 crystals. The second crystal was detuned by 50% to reduce the harmonic content of the beam. Monochromator position was calibrated using the pre-edge peak of TcO$_4^-$ adsorbed on ion exchange resin. Intensities of the incident and transmitted X-ray beam were measured using argon filled ion

chambers. Data were averaged using the software package SixPack, EXAFS data were obtained from the raw absorption data using Athena.{Ravel, 2005 #82}{Newville, 2001 #69} Data were deglitched to remove a large glitch (5 data points were deleted). EXAFS data were fit using Artemis. Theoretical scattering factors were calculated using Feff6 and the structural parameters for the complexes by modeling the scattering based upon the crystallographically determined structure for $H_3PW_{12}O_{40}$ by replacing one terminal W=O group with a ${TcX}^{3+}$.{Ankudinov, 1998 #4}

Electrochemical Data Collection. Electrochemical data were obtained using a BAS Voltammetric Analyzer System controlled by BAS CV-50W software (for PC). The cell used for cyclic voltammetry (CV) contained a glassy-carbon working electrode (BAS standard disk electrode, 3 mm OD), a Pt wire auxiliary electrode (0.5 mm), and a Ag/Ag^+ or Ag quasi reference electrode. For measurements conducted in acetonitrile, the reference electrode (BASi MF-2062) was constructed from a Ag wire immersed in a 0.1 mM $AgNO_3$ solution in acetonitrile containing 0.1 M tetrabutylammonium hexafluorophosphate. For ionic liquid studies the Ag wire was immersed in the non-aqueous electrode system containing neat ionic liquid, resulting in a quasi-reference electrode. The electrode was then stored under vacuum for 48 hours to ensure perfusion of the ionic liquid through the frit. Prior to obtaining electrochemical data, solutions were de-aerated for at least 30 minutes with high purity Nitrogen (N_2). Fine polishing of the glassy-carbon working electrode was adapted from the procedure of Keita and co-workers.[9]

Unless otherwise stated, scan rates were 100 mV/s, and experiments were carried at ambient temperatures under a N_2 atmosphere. All voltammograms presented are referenced versus the redox couple of Fc/Fc$^+$.

Collection of EPR Data.

Electron paramagnetic resonance (EPR) spectra were obtained at 2 K with a Varian E-12 spectrometer equipped with liquid helium cryostat, an EIP-547 microwave frequency counter, and a Varian E-500 gaussmeter, which was calibrated using 2,2-diphenyl-1-picrylhydrazyl (DPPH, g = 2.0036). The low temperature spectrum was fit using a version of the code ABVG[10] modified to fit spectra using the downhill simplex method.[11] The code was modified to use the modified to the Pilbrow lineshape, σ_{vi} given in eq 1[12] where g_i is the g-value, β is the Bohr magneton, H is the magnetic field, ν is the microwave frequency, A_i is the hyperfine coupling constant in cm^{-1}, σ_{Ri} is the residual linewidth, σ_{gi} is the g-strain, σ_{Ai} is the A-strain, and l_i is the direction cosine. Samples were sealed in a 1 mm ID quartz tube, which was sealed inside a 4 mm OD quartz tube.

$$\sigma_{vi}^2 = \sum_{i=1}^{3}\left[\sigma_{Ri}^2 l_i^2 + \left(\frac{\beta H g_i}{\upsilon g}\sigma_{gi} + M_I\frac{A_i g_i^2}{A g^2}\sigma_{Ai}\right)^2 l_i^4\right], \text{ where } g^2 = \sum_{i=1}^{3} g_i^2 l_i^2;\ A^2 = \sum_{i=1}^{3} A_i^2 g_i^2 l_i^2 \quad (1)$$

Synthesis of Compounds. TBA$_4$H$_3$[PW$_{11}$O$_{39}$] [13], TBA$_4$[Tc^{V}O-PW$_{11}$O$_{39}$] [6] (**1**) and TBA$_4$[Tc^{VI}N-PW$_{11}$O$_{39}$] [6] (**2**) were synthesized according to literature preparations. In the case of TBA$_4$[Tc^{V}O-PW$_{11}$O$_{39}$] extra steps were taken to

purify the target compound. In a typical preparation, 500 mg of crude TBA$_4$[Tc^{V}O-PW$_{11}$O$_{39}$] were precipitated from reaction mixture by the addition of an equal volume of diethyl ether. The crude product isolated by filtration was suspended in acetone (30 mL) and stirred for 30 minutes, filtered, and re-suspended and stirred a further 2 times. After the third acetone wash, the reside was stirred in dichloromethane containing TBAOH (30 mL, 70 mmol) for 30 minutes and the pure TBA$_4$[Tc^{V}O-PW$_{11}$O$_{39}$] isolated by filtration and recrystallized from acetonitrile. Impurities, namely TBA$_3$[PW$_{12}$O$_{39}$] and TBA$_4$H$_3$[PW$_{11}$O$_{39}$], from the crystallization of TBA$_4$[Tc^{VI}N-PW$_{11}$O$_{39}$] were mechanically separated from the target compound.

Oxidation of TBA$_4$[Tc^{V}O-PW$_{11}$O$_{39}$] to TBA$_3$[Tc^{VI}O-PW$_{11}$O$_{39}$] (3). 1 (200 mg, 0.05 mmol) was dissolved in dry acetonitrile (5 mL). Br$_2$ (200 μL, 7.7 mmol) was added to the acetonitrile solution of **1** under stirring. The reaction mixture turned from red/brown to orange-brown over a period of 30 minutes. The reaction was stirred overnight and crystalized through vapor diffusion of diethyl ether into the reaction solution.

Synthesis of Trimethylbutylammonium Bis(triflorormethanesulfonyl)imide (N1114-NTf$_2$)

Trimethylbutylammonium Iodide. Methyl Iodide, Alfa Aesar 99.5% (50 g, 0.35 mol) was added slowly to dimethylbutylamine (TCI 99%) (36 g, 0.35 mol) in an ice bath while stirring. The resultant solid suspension was slowly brought up to room temperature and stirred overnight. The resultant pale

yellow solid was isolated via vacuum filtration and dried under vacuum. The yellow solid was then dissolved in deionized water and 4 g (5% w/w) of activated charcoal was added to the solution. The solution was then heated to 65°C for 24 hours, cooled to room temperature and gravity filtered. The solution was rotary evaporated to yield a white solid. Yield 78 g, 0.32 mol 91%

Trimethylbutylammonium Bis(triflorormethanesulfonyl)imide (N1114-NTf$_2$). The trimethylbuytlammonium iodide (42 g, 0.17 mol) was dissolved in DI water (40 ml) and one molar equivalent of lithium bis(triflorormethanesulfonyl)imide (Acros Organics) was added to the stirring aqueous solution (50 g, 0.17 mol). The resultant IL was washed with deionized water to remove halide byproducts; adding a 50 mM silver nitrate solution to the washings detects the presence of any halide by precipitation of silver halide salts. The ionic liquid was dried using a vacuum oven for 2 days to achieve water content under 200 ppm. The ionic liquid was then stirred with DARCO charcoal (3% w/w) and filtered to remove fluorescent impurities. Yield 56 g, 0.14 mol 83%.

DFT Calculation parameters:

Results and discussion

For clarity, the discussion has been divided into two different sections: Structural characterization and Electronic characterization

Structural Characterization of complexes:

Multinuclear NMR. The ^{31}P NMR of **1** shows a single peak at -13.5 ppm in acetonitrile-d^3, attesting to the purity of the compound; a representative ^{31}P NMR spectrum is shown in **Figure 1**. ^{183}W NMR allows for the confirmation of the structure of the Cs symmetric α-Keggin structure. The C$_s$ symmery of the lacunary ion causes the ^{183}W resonances to be split into 6 signals that integrate to 2:2:2:2:2:1. In the case of **1,** the signals are also split into 6 signals with integrations of 2:1:2:2:2:2 (**Figure 2**). Upon the incorporation of {TcO}$^{3+}$ into the POM framework the ^{183}W resonances are diamagnetically shifted and retain integrations consistent with an α-Keggin structure, and a non-centrosymmetric Tc environment. The ^{31}P NMR of **2** is dominated by a broad resonance at -22 ppm, indicative of the interaction of the paramagnetic d^1 Tc^{VI} center with the internal phosphate. The spectrum also contains some small, sharp resonances at -12 and -15 ppm, which are due to an impurity from a diamagnetic **[Tc^{V}N-PW$_{11}$O$_{39}$]$^{4-}$** homologue.

X-Ray Absorption Fine Structure. The X-ray absorption near edge structure (XANES) spectra of **1, 2** and **3** are presented in **figure 7**. Each compound shows a well-defined pre-edge feature below 21050 eV, which is consistent with the non-centrosymmetric nature of these compounds. These features are due to the 1s-4d transition, which is symmetry forbidden in centrosymmetric complexes. The amount of screening of the 1s electrons is reflected by the positions of the rising edge half-heights. The energy at

which the edge appears is typically at a higher energy when the oxidation state is higher. This is can be complicated by the effects of covalency, which can shift the observed edge energy from what one would predict from oxidation state alone. Analysis of the half-height energies in **figure 7** relative to that of $[TcO_4]^-$ are -6, -9 and -5 eV for complexes **1**, **2**, and **3** respectively. This observation means that the effects of covalency are similar for the complexes containing the $\{TcO\}$ core; however, the $\{TcN\}^{3+}$ core displays greater screening of the Tc 1s electrons, presumably due to greater covalency in the Tc≡N bond relative to the Tc=O bond. Although isoelectronic to the O^{2-} ligand, N^{3-} is a potent π-electron donor and forms triple bonds with the Tc center, thus increasing the covalent nature of the $\{TcN\}^{3+}$ core within this complex. The Tc K-edge XANES spectrum of **1** is consisten with the +5 oxidation state and can be used as a standard for Tc^V within the framework of $[PW_{11}O_{39}]^{7-}$ for EXAFS studies of mineral surfaces.

Analysis of Tc K-edge Extended X-ray Absorption Fine Structure (EXAFS) spectra enables determination of the local environment around the technetium center. The Tc K-edge solution spectra and associated modeled spectra of **1**, **2** and **3** are shown in **figure 8**. The data were modeled using the single crystal structure for $[PW_{12}O_{40}]^{3-}$ [14] (**PW₁₂**). A single tungsten atom was replaced with a single technetium atom. The data was fit using the shell-by-shell approach, sequentially adding atoms at increasing distances from the Tc center. The added scattering shells were kept if reduced χ-squared

decreased. The number of heavy atom (W and P) neighbors and number of nearest O and N atoms were determined from the crystallographic model, but the number of distant scatterer atoms were varied to obtain the best fit. The local structures determined from the fits are summarized in **table 2** and detailed fit parameters can be found in the **ESI**. The EXAFS fit parameters of all complexes are consistent with the local structure of a {TcX} core replacing a W=O group in PW_{12}. All atoms used in the fits contribute significantly to the spectra as shown by an F-test, and the salient points of the EXAFS fits are discussed below.

TBA$_4$[Tc^{V}O-PW$_{11}$O$_{39}$] (1). The second shell of 5 oxygen atoms fits equally well with 4 oxygen atoms. The Tc=O bond length is observed to be shorter than our W=O model (1.65 Å), which is typical for ${Tc=O}^{3+}$ cores.

TBA$_4$[Tc^{VI}N-PW$_{11}$O$_{39}$] (2). Fitting the second shell with 5 oxygens (4 arising from the POM and one from an internal phosphate) does not significantly improve the fit. The short 1.63 Å TcN bond is typical for such systems<mark>[needs a reference]</mark>. Exclusively modeling the internal phosphate oxygen as a separate shell was difficult and did not improve the overall fit and the large Debeye-Waller factors indicated disorder. The position of the phosphorous atom however is well defined and can be seen to contribute to the scattering with a high probability.

TBA$_3$[Tc^{VI}O-PW$_{11}$O$_{39}$] (3). We found that fitting the second shell with 5 oxygen atoms (4 arising from the POM and one from an internal phosphate) significantly worsens the fit. The short 1.65 Å TcO bond is typical for such

systems and is identical to the bond length in the Tc^VO complex. The distance from the scattering from the oxygen atom of the phosphate suggests that the Tc^{VI} atom is pulled into the vacancy by approximately 0.10(3) Å.

Comparison of complexes

Regarding complexes containing Tc=O. There are 3 main observations comparing **1** and **3**. 1) The Tc=O bond length does not appear to change upon oxidation. 2) The average Tc-O bond length, including the equatorial Os and the O trans to the terminal oxo, increases upon oxidation from Tc^V to Tc^{VI}. 3) The Tc-W distances remain essentially identical.

For this to make sense we need to consider what we can see via the EXAFS in comparison with the bond distances observed in our **PW$_{12}$** model. In both cases (**1** & **3**) the Tc-W distances are smaller in the TcO complexes relative to W-W distances the parent α-Keggin ion. This difference illustrates that Tc is pulled into the POM framework. In tandem with this, we can fit the Tc-O-P distance in the $Tc^{VI}O$ complex, which is shorter than in **PW$_{12}$** and the equatorial Tc-O distances are also shorter than with a W in the structure. Unfortunately we do not observe scattering from the P atom or an individual O from the phosphate in complex **1**. However, based on the average of the Tc-O bonds (excluding the terminal oxo) would imply that it is pulled in further than the Tc(VI)O by 0.05 Å.

Regarding complexes containing {TcN}. The Tc-W distances in complex

2 *are similar to the oxo examples yet we can model the P atom. While the Tc-W distances are significantly shorter in the Tc complex compared to the W-W distances in the XRD, the Tc-P distance is the same. The Tc-O bond lengths are longer too, which would imply that the O atoms are being pushed away from the Tc center without altering the geometry too much i.e. making the O-W bonds shorter somehow.*

Table comparing the observed bond lengths from the EXAFS data and the calculated bond lengths via DFT.

Bond	PW$_{12}$			Tc$^{(V)}$O-PW$_{11}$			Tc$^{(VI)}$O-PW$_{11}$			TcN-PW$_{11}$		
	Bond Length (Å cif)	Bond Length (Å DFT)	Difference	Bond Length (Å EXAFS)	Bond Length (Å DFT)	Difference	Bond Length (Å EXAFS)	Bond Length (Å DFT)	Difference	Bond Length (Å EXAFS)	Bond Length (Å DFT)	Diffference
M=O	1.72	1.698	0.022	1.65	1.649	0.001	1.65	1.655	-0.005	1.631	1.621	0.01
M-O	1.908	1.905	0.003	1.962	1.916	-0.0728[a]	1.904	1.882	0.013[b]	1.998	1.944	0.048[b]
M-O	1.899	1.896	0.003		1.936			1.9			1.956	
M-O-P	2.416	2.411	0.005		2.47		2.38	2.429	-0.049		2.497	
M-P	3.556	3.55	0.006		3.605			3.557		3.67	3.595	-0.075
M-W	3.405	3.394	0.011	3.43	3.404	0.026	3.427	3.398	0.029	3.43	3.397	-0.033
M-W	3.704	3.678	0.026	3.71	3.659	0.051	3.71	3.665	0.045	3.78	3.671	0.109

[a] The EXAFS showed 5 nearest neighboring O atoms, difference is based on the average of the 4 M-O bonds plus an O atom from the phosphate in the DFT-optimized structure

[b] The EXAFS showed 4 nearest neighboring O atoms, difference is based on the average of the 4 M-O bonds from the DFT-optimized structure

Electronic Characterization of complexes

Density Functional Theory

In order to explore the possible oxidation states of technetium we turned to theoretical means to generate the different redox species. Each structure geometry was optimized before calculating spin densities and relative energy levels. The energy levels of Tc^V and Tc^{VI} complexes are presented in **figure 6**, and the electronic structure parameters summarized in tables Y and Z. The calculated frontier orbital diagram shows that removing an electron from $\{Tc^VO\}^{3+}$ to form $\{Tc^{VI}O\}^{4+}$ lowers the overall energy of the system. Normally associated with an increase in overall stability this energy difference causes the Tc center to be more susceptible to reduction and therefore, less stable. In other words, the $Tc^{VI}O$ incorporated into the POM framework is easily reduced and not stable. We will take a look at each core to compare their electronic properties and use this to assign redox waves;

Tc^VO. The HOMO of **1** has 52% Tc character. Addition of an electron into the system is likely to result in the reduction of Tc^V to Tc^{IV} as the LUMO is predominantly Tc-based (53%). The LUMO also possesses some terminal oxygen character. Further additions of electrons are likely to go into Tc-based orbitals, potentially producing a Tc^{III}-baring system before a "blue" reduced tungsten species. Oxidation of the Tc center results in a Tc^{VI} system where the electrons are unpaired. Analysis of the spin densities show that the electron resides predominantly on the Tc. Reduction is thus likely to

occur in the Tc d orbital (the Tc-Beta). This agrees with experimental observations vide infra.

Tc^{VI}N. Addition of electrons can theoretically go into the beta-Tc orbital or the W-based LUMO+1 orbital. The calculated spin densities for the system show that 68% resides on the Tc center, which would mean that any reduction would result in a Tc^V and not a reduced heteropoly blue species. Unlike the TcO system, the addition of further electrons are predicted to go into W-based orbitals, so a Tc^{IV} or Tc^{III} is theoretically unlikely to occur with the {TcN} core.

Cyclic voltammetry

Cyclic voltammetry in organic solution. Cyclic voltammetry of 0.25 μM solutions of **1** and **2** in acetonitrile containing 0.1 M TBAPF$_6$ are shown in **figure 4**. The redox waves c.a. -1.88 V are due to redox processes of the tungsten framework. The Tc^{V}O (red trace) shows three reversible redox waves centered at -0.94, +0.38 and +1.30 V and have been assigned to Tc$^{IV/V}$, Tc$^{V/VI}$, and Tc$^{VI/VII}$ redox reactions respectively. The Tc^{VI}N (blue trace) shows 2 reversible redox waves c.a. -0.44 and +0.79 V and have been assigned to Tc$^{V/VI}$ and Tc$^{VI/VII}$ reactions respectively.

The Tc^V within the {TcN}$^{2+}$ core is more easily oxidized than the Tc^V within the {TcO}$^{3+}$ core by 0.83 V, which tracks with the N^{3+} ligand's ability to stabilize higher Tc oxidation states through π-donation. Comparatively, the

Tc^{IV} oxidation state is seen to be accessible in the TcO core, which comments on the ability of the oxo core to stabilize low oxidation states.

Cyclic voltammetry in ionic liquids. Ionic liquids are attractive media for electrochemical studies as they can act as both the solvent and supporting electrolyte. Ionic liquids also tend to have low vapor pressure, high thermal stability and wide electrochemical windows. Electrochemical studies in ionic liquids have shown that redox processes tend to be shifted towards positive potential and may provide ways to access uncommon oxidation states of metal ions[ref]. **Figure 5** shows cyclic voltammagrams for **1** and **2** adhered to glassy carbon working electrodes immersed in the ionic liquid **N1114-NTF$_2$**. Solubility of complexes **1** and **2** in **N1114-NTf$_2$** is poor (<0.1 mg/mL) and precludes meaningful electrochemical studies in our hands. We used a modified method of dropcasting[ref] to increase the concentration of **1** and **2** near the electrode surface and circumvent problems associated with poor mass transport at low concentrations of analyte in the ionic liquid. Both complexes show waves at -1.8 V attributed to W-centered phenomena. The Tc^{V}O (red trace **Fig. 5**) shows three reversible redox waves centered at -0.57, +0.66 and +1.40 V and have been assigned to Tc$^{IV/V}$, Tc$^{V/VI}$, and Tc$^{VI/VII}$ redox respectively. The Tc^{VI}N (blue trace **Fig. 5**) shows 2 reversible waves at -0.05 and +1.05 V and have been assigned to Tc$^{V/VI}$ and Tc$^{VI/VII}$ redox respectively.

Comparison of electrochemistry in acetonitrile vs ionic liquid. The electrochemistry of **1** and **2** is dependent on electrolyte. $Tc^{IV/V}$, $Tc^{V/VI}$ and $Tc^{VI/VII}$ redox waves are respectively 370, 320 and 200 mV more positive in the ionic liquid on average, which indicates that Tc reduction is more facile in **N1114-NTF₂** vs 0.1 M TBAPF₆ in acetonitrile. Interestingly the difference between the redox behavior of the two $\{TcX\}^{3+}$ cores is less pronounced in the ionic liquid. The $\{TcO\}^{3+}$ core can be reduced more easily than the $\{TcN\}^{2+}$ core by 0.83 V in acetonitrile vs 0.71 V in **N1114-NTF₂**. Both compounds show a new redox wave c.a. -1.3 mV in **N1114-NTF₂** that is not observed in the acetonitrile system. We have assigned this to W-centered redox phenomena. POM redox is highly sensitive to the environment in which it is studied and is influenced by pH and counterion concentration. It is likely that **N1114-NTF₂** shifts W-centered redox waves to more positive potential similar to the Tc redox waves. Along with the positive shift of all redox potentials, the Tc-centered voltammetry of the complexes in **N1114-NTF₂** occurs in a smaller electrochemical window relative to acetonitrile.

EPR spectra of 2 and 3. Stirring an acetonitrile solution of **1** in the presence of bromine or thianthrinium BF₄ (**ESI**) produces **3**. X-band EPR spectra of the Tc^{VI} complexes were taken at 1.5 K. The EPR spectra show >10 lines due to hyperfine splitting consistent with the 9/2 nuclear spin of [99]Tc. The spectra of **2** and **3** are shown in **figure 9** (individual spectra are given Sxx to Szz in the **ESI**) and summarized in **tables 5**. For both **2** and **3**, the EPR spectra can be accurately simulated with the exception of the region

around 2900 Oe in **3**, which is due to an angular anomaly and was given zero weight during the fitting.{Abragam, 1970 #119} The EPR signals in **2** and **3** unequivocally demonstrate that these complexes contain predominantly Tc^{VI}. The spectral parameters may be assigned on the basis of the hyperfine coupling constants (A values) since the coupling constant along the Tc=X axis is much larger than that perpendicular to Tc=X axis. As shown in Table 5, **2** and **3**, are close to axially symmetric but actually posses lower symmetry consistent with the C_s symmetry of the Tc center. For the following discussion, the average perpendicular g and A values are used.

Defining the z-axis along Tc=X, and the x- and y-axes along the equatorial Tc-O bonds the unpaired electron occupies the d_{xy} orbital. The hyperfine coupling constants are closely related to the metal character of the singly occupied molecular orbital (SOMO), which may be quantified from the g- and A-values if the value of $P = g_e g_N \beta_e \beta_N \langle r^{-3} \rangle$, where g_e and g_N are the g-values of the electron and nucleus, respectively, and the Bohr and nuclear magnetons are represented by β_e β_N, and $\langle r^{-3} \rangle$ is the expectation value of r^{-3}, which may be determined by Hartree-Fock calculation. {McGarvey, 1967 #115} For Tc(VI), the value of P is extrapolated to be 0.0293 cm^{-1} from the values of $\langle r^{-3} \rangle$ for Tc(II) and the averaged oxidation state dependence of $\langle r^{-3} \rangle$ for Mo and Ru. {Freeman, 1965 #117} Using this value, the Tc character of **2** and **3** is 58% and 56%, which is slightly larger than that calculated by DFT. The Tc character in **2** and **3** may be compared to that of $[Cl_5Tc^{VI}=O]^-$ and

[Cl$_4$Tc^{VI}=N]$^-$, which are somewhat larger, 77% and 81%, respectively.{Abram, 1988 #116}

The g-values of **2** and **3** provide information about the energies of low-lying excited states since the decrease of the g-values relative to g$_e$ (2.0023) is due to spin-orbit coupling to unoccupied excited states.{McGarvey, 1966 #118} Most significantly, the change in g$_\perp$ is inversely proportional to the energy of the the d$_{zx}$, d$_{yz}$ orbitals, which are π-antibonding with respect to Tc=X. The energy gap cannot be quantified for **2** and **3** since the number of unknown parameters exceeds the available data. However, the greater deviation of g$_\perp$ in **2** relative to **3** can be qualitatively attributed to greater destabilization of the d$_{zx}$, d$_{yz}$ orbitals in **2** due to stronger π-(anti)bonding between Tc and its terminal nitrido ligand relative to that of a terminal oxo ligand. This difference in bonding is also reflected in the LUMOs determined by DFT and shown in Figure 6. In **2,** the LUMO is d$_{zx}$, d$_{yz}$ while in **3**, the stronger π bonding to nitride results in greater destabilization of these orbitals such that a non-degenerate orbital is the LUMO.

Conclusions

We have revisited the synthesis and characterization of technetium complexes with $[PW_{11}O_{40}]^{7-}$ and have shown that the Tc within the tungsten framework can be oxidized with bromine or thianthrenium BF_4 to make a $Tc^{VI}=O$. Comparison with the TcN complex shows that the Tc is more easily oxidized in comparison to the TcO complex. The purity and structural characterization of the complexes can be used as a molecular level model for Tc^V bound to mineral phases and can be used as standards for modeling Tc^V and Tc^{VI} in those environments.

FIGURE CAPTIONS

Figure 1. ^{31}P NMR of **1** in d^{3}MeCN

Figure 2. ^{183}W NMR of TBA$_4$H$_3$PW$_{11}$O$_{40}$ and **1** in d^{3}MeCN (300 mg/mL)

Figure 3. ^{31}P NMR of **2** in d^{3}MeCN

Figure 4. Cyclic voltammetry of 0.2 mM solutions of **1** and **2** in MeCN containing 0.1 M TBAPF$_6$ supporting electrolyte. Scan rate = 100 mVs^{-1}

Figure 5. Cyclic voltammetry of dropcast **1** and **2** in N1114NTF2. Scan rate = 100 mVs^{-1}

Figure 6. Calculated molecular orbital diagram. The HOMO is represented by a circle for each electron in the molecular orbital. Molecular orbital visualizations a) TBA$_4$[Tc^{V}O-PW$_{11}$O$_{39}$] HOMO b) TBA$_4$[Tc^{V}O-PW$_{11}$O$_{39}$] LUMO c) TBA$_4$[Tc^{VI}N-PW$_{11}$O$_{39}$] HOMO d) TBA$_4$[Tc^{VI}N-PW$_{11}$O$_{39}$] LUMO.

Figure 7. XANES of **1, 2** and **3**.

Figure 8. EXAFS of **1, 2** and **3**.

Figure 9. EPR of **2** and **3;** the sharp feature at 2900 Oe is an angular anomaly and this region omitted during least squares fitting.

Figure 10. EPR of **2;** the sharp feature at 2900 Oe is an angular anomaly and this region omitted during least squares fitting.

Figure 11. EPR of **3** made in situ with Br$_2$

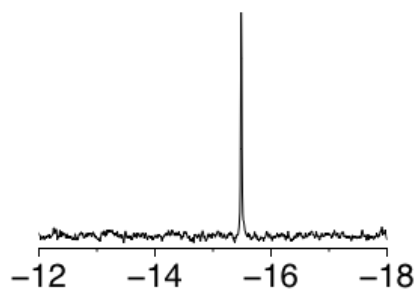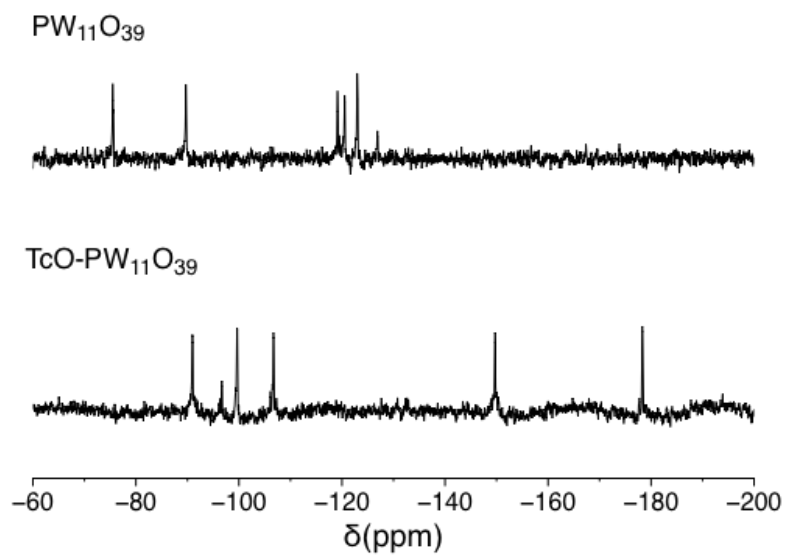**Figure 12.** EPR of **3** made in situ with BF$_2$

Figure 1.
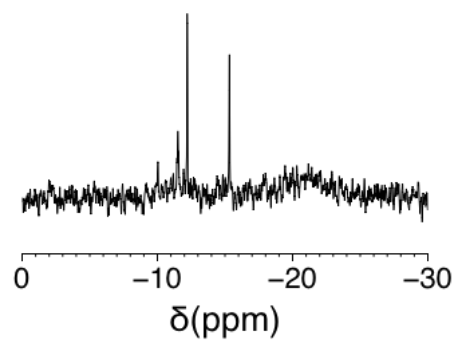
Figure 2.

$PW_{11}O_{39}$

$TcO-PW_{11}O_{39}$

δ(ppm)

Figure 3.

δ(ppm)
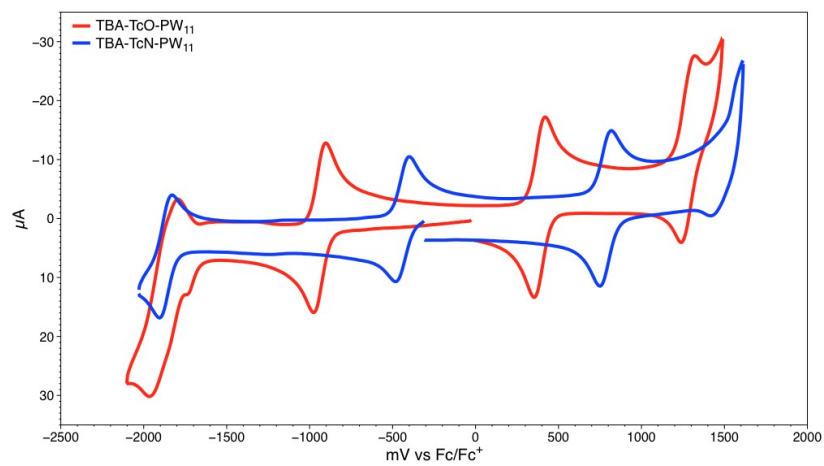
Figure 4.

Figure 5.

Figure 6.

a)   b)

c)

d)
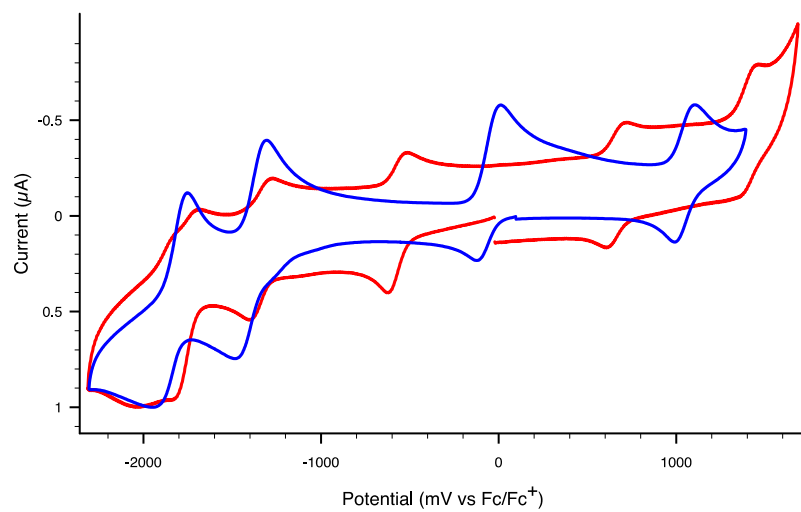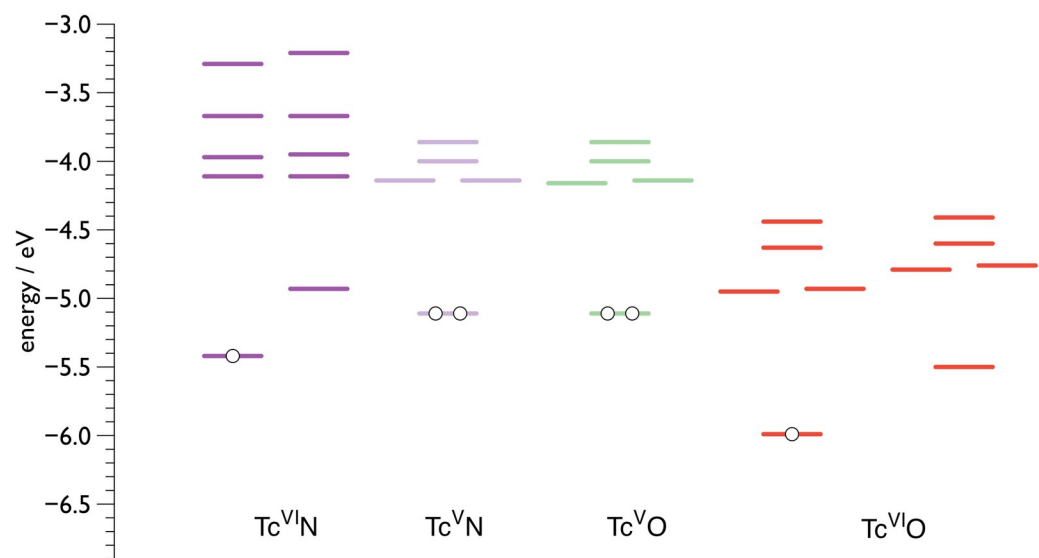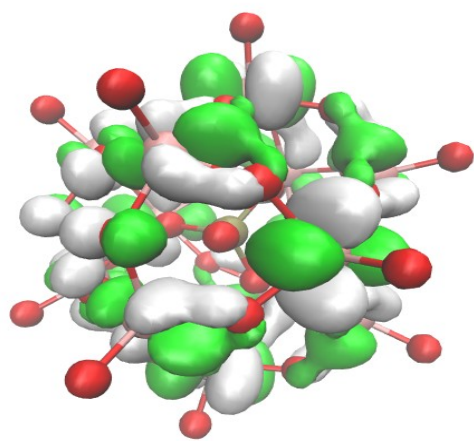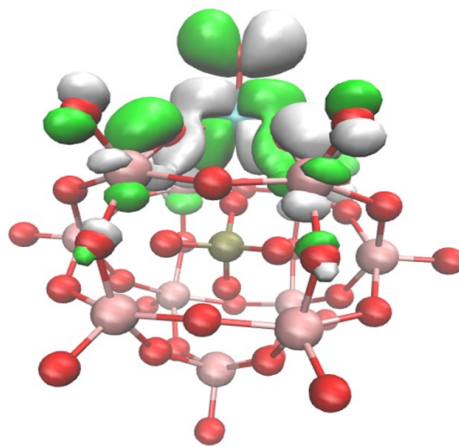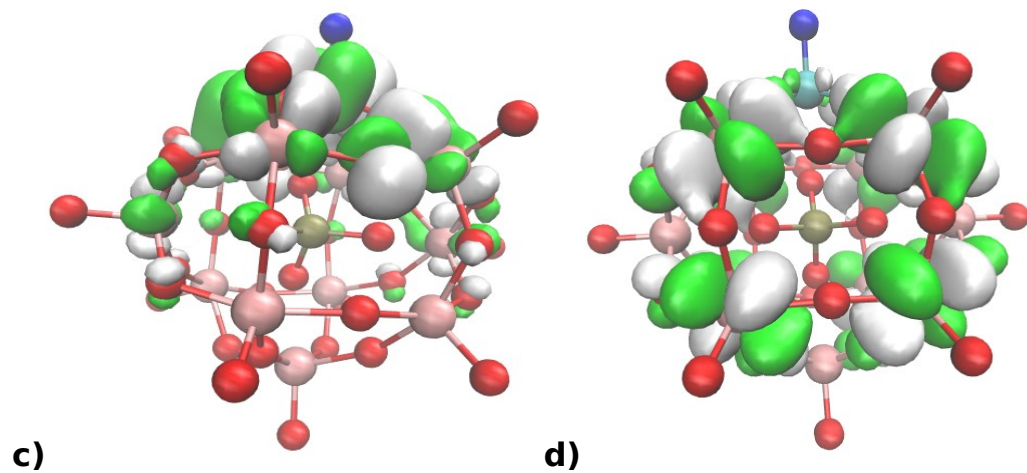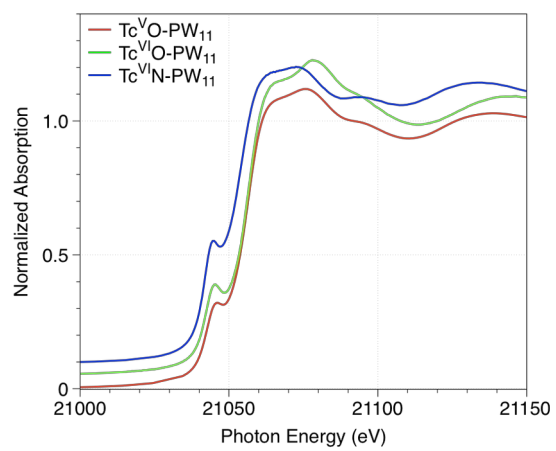
Figure 7.

Figure 8.

Figure 9.

Figure SIxx

Figure SIyy
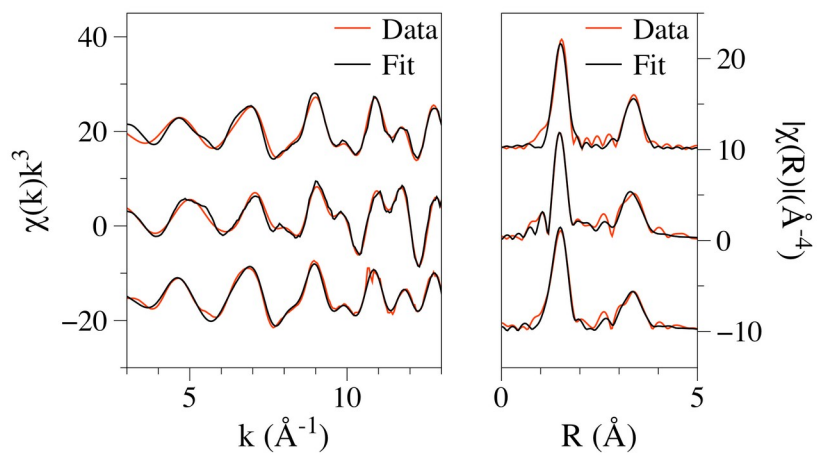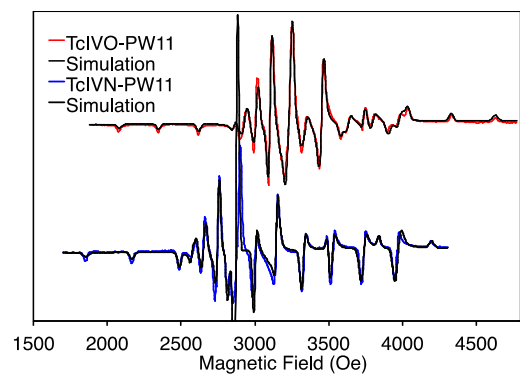
Figure SIzz

TABLES.

Table 1.

ESI-MS data is not great Maybe put in ESI

Table Y. Electronic structure parameters for **1** and **3**

	1 {Tc^{V}O}$^{3+}$			**3** {Tc^{VI}O}$^{4+}$					
	Tc	O	POM	Tc(α)	Tc(β)	O(α)	O(β)	POM(α	POM(β

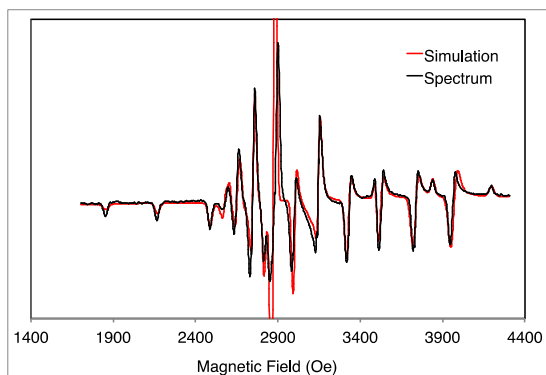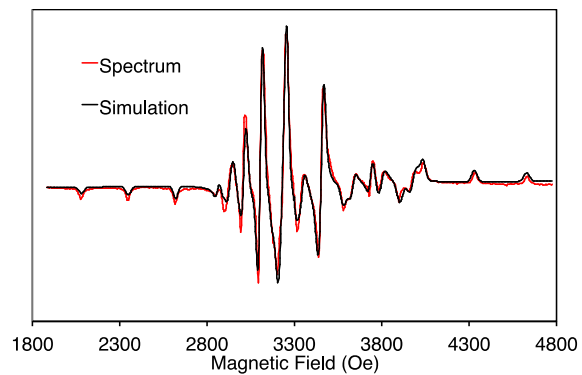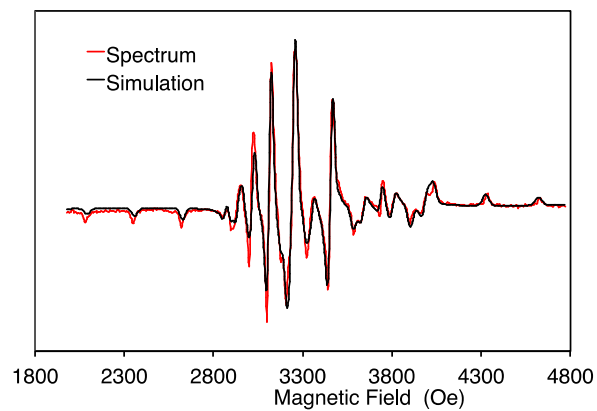|	4 $\{Tc^V N\}^{2+}$			2 $\{Tc^{VI} N\}^{3+}$					
	Tc	N	POM	Tc(α)	Tc(β)	N(α)	N(β)	POM(α)	POM(β)
Charges	1.49	-0.39	-2.88	1.58		-0.35		-1.77	
MO(%)									
HOMO	52			47					
LUMO	53	22			49				
LUMO+1	52	21		50		24			
LUMO+2			10		52		20		
LUMO+3			39	49		23			

Table Z. Electronic structure parameters for **2** and **4**

	4 $\{Tc^V N\}^{2+}$			2 $\{Tc^{VI} N\}^{3+}$					
	Tc	N	POM	Tc(α)	Tc(β)	N(α)	N(β)	POM(α)	POM(β)
Charges	1.49	-0.39	-2.88	1.58		-0.35		-1.77	
MO(%)									
HOMO	47			52					
LUMO			13		52				
LUMO+1			27					20	
LUMO+2			13						22
LUMO+3			13					25	

Table a. Spin densities

Core	Tc	N/O	POM
$\{Tc^{VI}O\}^{4+}$	0.61	-0.044	0.43
$\{Tc^{VI}N\}^{3+}$	0.68	-0.076	0.4

Table 2. Table comparing the observed EXAFS fits with the initial PW_{12} model. M= W or Tc.

Bond	Number	PW$_{12}$ Distance (Å)	Tc$^{(V)}$O-PW$_{11}$ Distance (Å)	Tc$^{(V)}$O-PW$_{11}$ Deviation from PW$_{12}$	Tc$^{(VI)}$O-PW$_{11}$ Distance (Å)	Tc$^{(VI)}$O-PW$_{11}$ Deviation from PW$_{12}$	TcNPW$_{11}$ Distance (Å)	TcNPW$_{11}$ Deviation from PW$_{12}$
M=O	1	1.72	1.65	-0.07	1.65	-0.07	1.631	-0.089
M-O	2	1.908	1.962	-0.044[a]	1.904	0.0005[b]	1.998	0.0945[b]
M-O	2	1.899						
M-O-P	1	2.416			2.38	-0.036		
M-P	1	3.556					3.67	0.114
M-W	2	3.405	3.43	0.025	3.427	0.022	3.43	0.025
M-W	2	3.704	3.71	0.006	3.71	0.006	3.78	0.076

[a] The EXAFS showed 5 nearest neighboring O atoms, difference is based on the average of the 4 M-O bonds plus an O atom from the phosphate in the model

[b] The EXAFS showed 4 nearest neighboring O atoms, difference is based on the average of the 4 M-O bonds in the model

Table 5. Selected EPR simulation parameters for **2** and **3**

Axis	**2** g_i	**2** A_{ii} (10^{-4})	**3** g_i	**3** A_{ii} (10^{-4})
‖	1.98	145	1.90	110
	1.98	138	1.91	108
	1.93	307	1.96	252
	1.98	142	1.91	109
⊥ (av)				

Table SIxx.

EPR simulation parameters for $PW_{11}TcN$ (**2**)

Axis (i)	g_i	A_{ii} $(10^{-4}$ $cm^{-1})$	A_{12},A_{13},A_{23} $(10^{-4}$ $cm^{-1})$	σ_{Ri} (Oe)	σ_{gi} (Oe)	σ_{Ai} (Oe)
1	1.983	145	1	5.65	-5.63	0.59
2	1.983	138	-12	5.65	-5.63	0.59
3	1.931	307	-7	8.88	0.000	3.96

Table SIyy.

EPR simulation parameters for **3** from **1** + Br_2

Axis (i)	g_i	A_{ii} $(10^{-4}$ $cm^{-1})$	A_{12},A_{13},A_{23} $(10^{-4}$ $cm^{-1})$	σ_{Ri} (Oe)	σ_{gi} (Oe)	σ_{Ai} (Oe)
1	1.906	110	4	11.28	1.63	1.95
2	1.918	108	5	11.28	1.63	1.95
3	1.960	252	31	12.84	0.77	1.69

Table SIzz.

EPR simulation parameters for **3** from **1**+ Thianthrenium BF_4

Axis (i)	g_i	A_{ii} $(10^{-4}$ $cm^{-1})$	A_{12},A_{13},A_{23} $(10^{-4}$ $cm^{-1})$	σ_{Ri} (Oe)	σ_{gi} (Oe)	σ_{Ai} (Oe)
1	1.903	109	5	11.04	1.89	1.52
2	1.917	106	7	11.04	1.89	1.52
3	1.958	252	26	12.90	0.15	2.73

Displayed equations can be inserted where desired making sure they are assigned Word Style "Normal". Displayed equations can only be one column

wide. If the artwork needs to be two columns wide, it must be relabeled as a figure, chart, or scheme and mentioned as such in the text.

ASSOCIATED CONTENT

(Word Style "TE_Supporting_Information"). **Supporting Information**. A brief statement in non-sentence format listing the contents of material supplied as Supporting Information should be included, ending with "This material is available free of charge via the Internet at http://pubs.acs.org." For instructions on what should be included in the Supporting Information, as well as how to prepare this material for publication, refer to the journal's Instructions for Authors.

AUTHOR INFORMATION

Corresponding Author

*To whom correspondence should be addressed. Email:
benjamin.burtonpye@lehman.cuny.edu, lfrances@hunter.cuny.edu

Present Addresses

†Department of Chemistry and Biochemistry, University of Notre Dame, 301 Stinson-Remick Hall, Notre Dame, IN 46556.

Notes

Any additional relevant notes should be placed here.

ACKNOWLEDGMENT

ABBREVIATIONS

TBA, tetrabutyl ammonium;

REFERENCES

(Word Style "TF_References_Section"). References are placed at the end of the manuscript. Authors are responsible for the accuracy and completeness of all references. Examples of the recommended format for the various reference types can be found at http://pubs.acs.org/page/4authors/index.html. Detailed information on reference style can be found in *The ACS Style Guide,* available from Oxford Press.

Insert Table of Contents Graphic and Synopsis Here.

(1)   Day, V. W.; Klemperer, W. G. *Science* **1985**, *228*, 533.

(2)   Day, V. W.; Klemperer, W. G.; Schwartz, C.; Wang, R.-C. In *Surface Organometallic Chemistry: Molecular Approaches to Surface Catalysis*; Kluwer Academic Publishers: New York, 1988, p 173.

(3)   Fang, X.; Hill, C. L. *Angew. Chem. Int. Ed.* **2007**, *46*, 3877.

(4)   Long, D.-L.; Burkholder, E.; Cronin, L. *Chem. Soc. Rev.* **2007**, *36*, 105.

(5)   Burton-Pye, B. P.; Radivojevic, I.; McGregor, D.; Mbomekalle, I. M.; Lukens, W. W., Jr.; Francesconi, L. C. *Journal of the American Chemical Society* **2011**, *133*, 18802.

(6)   Abrams, M. J.; Costello, C. E.; Shaikh, S. N.; Zubieta, J. *Inorganica Chimica Acta* **1991**, *180*, 9.

(7)   Boyd, G. E. *Journal of Chemical Education* **1959**, *36*, 3.

(8)   Davison, A.; Trop, H. S.; Depamphilis, B. V.; Jones, A. G. *Inorganic Syntheses* **1982**, *21*, 160.

(9)   Keita, B.; Girard, F.; Nadjo, L.; Contant, R.; Belghiche, R.; Abbessi, M. *Journal of Electroanalytical Chemistry* **2001**, *508*, 70.

(10)   Daul, C.; Schlapfer, C. W.; Mohos, B.; Ammeter, J.; Gamp, E. *Comp. Phys. Commun.* **1981**, *21*, 385.

(11)   Press, W. H.; Teukolsky, S. A.; Vetterling, W. T. *Numerical Recipes in Fortran 77: The Art of Scientific Computing*; Cambridge University Press: Cambridge, 1992.

(12)   Pilbrow, J. R. *Transition Ion Electron Paramagnetic Resonance*; Clarendon Press: Oxford, 1990.

(13)   Radkov, E.; Beer, R. H. *Polyhedron* **1995**, *14*, 2139.

(14)   Brown, G. M.; Noespirlet, M. R.; Busing, W. R.; Levy, H. A. *Acta Crystallographica Section B-Structural Science* **1977**, *33*, 1038.